European Heart Journal (2011) **32**, 104–114
doi:10.1093/eurheartj/ehq345

Head-to-head comparison of contrast-enhanced magnetic resonance imaging and electroanatomical voltage mapping to assess post-infarct scar characteristics in patients with ventricular tachycardias: real-time image integration and reversed registration

Adrianus P. Wijnmaalen[1], Rob J. van der Geest[2], Carine F.B. van Huls van Taxis[1], Hans-Marc J. Siebelink[1], Lucia J.M. Kroft[3], Jeroen J. Bax[1], Johan H.C. Reiber[2], Martin J. Schalij[1], and Katja Zeppenfeld[1]*

[1]Department of Cardiology, Leiden University Medical Center, Postbus 9600, 2300 RC, Leiden, The Netherlands; [2]Division of Image Processing, Department of Radiology, Leiden University Medical Center, Leiden, The Netherlands; and [3]Department of Radiology, Leiden University Medical Center, Leiden, The Netherlands

Received 9 February 2010; revised 10 July 2010; accepted 30 July 2010; online publish-ahead-of-print 23 September 2010

See page 16 for the editorial comment on this article (doi:10.1093/eurheartj/ehq357)

Aims Substrate-based ablation of ventricular tachycardia (VT) relies on electroanatomical voltage mapping (EAVM). Integration of scar information from contrast-enhanced magnetic resonance imaging (CE-MRI) with EAVM may provide supplementary information. This study assessed the relation between electrogram voltages and CE-MRI scar characteristics using real-time integration and reversed registration.

Methods and results Fifteen patients without implantable cardiac defibrillator (14 males, 64 ± 9 years) referred for VT ablation after myocardial infarction underwent CE-MRI. Contours of the CE-MRI were used to create three-dimensional surface meshes of the left ventricle (LV), aortic root, and left main stem (LM). Real-time integration of CE-MRI-derived scar meshes with EAVM of the LV and aortic root was performed using the LM and the CARTO surface registration algorithm. Merging of CE-MRI meshes with EAVM was successful with a registration error of 3.8 ± 0.6 mm. After the procedure, voltage amplitudes of each mapping point were superimposed on the corresponding CE-MRI location using the reversed registration matrix. Infarcts on CE-MRI were categorized by transmurality and signal intensity. Local bipolar and unipolar voltages decreased with increasing scar transmurality and were influenced by scar heterogeneity. Ventricular tachycardia reentry circuit isthmus sites were correlated to CE-MRI scar location. In three patients, VT isthmus sites were located in scar areas not identified by EAVM.

Conclusion Integration of MRI-derived scar maps with EAVM during VT ablation is feasible and accurate. Contrast-enhanced magnetic resonance imaging identifies non-transmural scars and infarct grey zones not detected by EAVM according to the currently used voltage criteria and may provide important supplementary substrate information in selected patients.

Keywords Myocardial infarction • Catheter ablation • Tachyarrhythmias • Magnetic resonance imaging • Mapping

* Corresponding author. Tel: +31 715262020, Fax: +31 715266809, Email: k.zeppenfeld@lumc.nl

Introduction

Catheter ablation is an important therapeutic option for recurrent ventricular tachycardia (VT) in patients late after myocardial infarction (MI).[1] The majority of these patients are inducible for VTs not suitable for mapping during tachycardia.[2,3] Substrate-based methods have been developed to identify ablation target sites during sinus rhythm.[2,4] These methods rely on the delineation of myocardial scar by electroanatomical voltage mapping (EAVM).

Contrast-enhanced magnetic resonance imaging (CE-MRI) can be used to visualize the three-dimensional (3D) geometry of myocardial fibrosis and is the gold standard for the detection of non-transmural scar.[5,6] Scar heterogeneity on CE-MRI based on signal intensity (SI) has been associated with spontaneous and inducible VT.[7,8] Furthermore, animal studies showed that CE-MRI-defined scar geometry can predict the location of VT reentry circuits.[9] Thus, the integration of CE-MRI-derived scar information with EAVM may provide important additional information to facilitate VT ablation procedures. Recently, post-MI scar areas delineated by CE-MRI have been shown to correspond with scar areas defined by EAVM. In two studies, different voltage cut-off values were reported to discriminate between the presence and the absence of scar based on a post-procedural image comparison.[10,11] However, a single-voltage cut-off value for the presence of scar may not reflect the complex scar architecture and its use may not result in accurate delineation of non-transmural scar and infarct grey zones.

The purpose of the present study was (i) to show the feasibility and accuracy of real-time integration of CE-MRI-derived scar maps and EAVM in post-MI patients. Mapping was performed with emphasis on scar border zone, non-transmural infarcts, and grey zones as assessed by CE-MRI. (ii) Then using a post-procedural process, bipolar and unipolar voltages of each mapping point were compared with scar transmurality and SI of the corresponding CE-MRI segment. (iii) Finally, the correlation between VT reentry circuit isthmus sites and CE-MRI scar locations was determined.

Methods

Fifteen consecutive patients referred for catheter ablation of sustained monomorphic VT late after MI without contraindication for MRI were studied. In three patients, the indication for ablation was VT that could not be controlled by antiarrhythmic drugs. In 12 patients with a reasonably preserved ejection fraction, radiofrequency (RF) ablation procedure was offered as an alternative for amiodarone therapy or implantable cardioverter defibrillator (ICD) implantation. Informed consent was obtained from all patients. No Ethics Committee approval was obtained as all performed procedures were part of the routine clinical protocol applied at the Leiden University Medical Center.

Magnetic resonance imaging acquisition and processing

Magnetic resonance imaging was performed on a 1.5 T Gyroscan ACS-NT/Intera MR system (Philips Medical Systems, Best, The Netherlands) with patients positioned in the supine position. A standardized clinical cardiac MRI protocol was followed, including cine MRI in long-axis (two- and four-chamber views) and short-axis orientation covering the complete left ventricle (LV). In addition, the proximal aorta including the ostium of the left main coronary artery (LM) and the right coronary artery was imaged in a stack of cross-sectional slices using a black-blood turbo spin-echo sequence. Contrast-enhanced images were acquired 15 min after bolus injection of gadolinium using an imaging protocol as described previously.[8] The heart was imaged in one breath-hold with 20–24 imaging levels (dependent on heart size) in short- and long-axis views. Images were acquired 600–700 ms after the R-wave on surface electrocardiogram.

Image analysis was performed using in-house-developed software (Mass research software, V2008-EXP). In the aorta image series, contours were traced describing the lumen of the aorta and the centreline of the LM and the proximal right coronary artery. In the CE short-axis image series, LV endocardial, LV epicardial, and right ventricular (RV) endocardial contours were manually traced (*Figure 1A*). Myocardial tissue with an SI value of $\geq$35% of the maximum SI within the infarct region was considered scar. The infarct core was defined as a myocardium with an SI of $\geq$50 and infarct grey zone as a myocardium with SI $\geq$35% but SI $<$50% of the maximum SI (*Figure 1B*).[8] Transmurality of scar was computed for every location for different layers within the LV myocardium. Subsequently, the LV anatomy as described by the endocardial and epicardial contours was converted into 3D mesh files that could be imported into the CARTO system (Biosense Webster, Cordis-Webster, Johnson & Johnson, Diamond Bar, CA, USA). Three-dimensional meshes were constructed by converting the traced myocardial and aorta contours into 3D co-ordinates, based on the 3D spatial location and pixel size of the MR images. Assuming minimal patient motion between the various MR sequences, the generated meshes are spatially aligned in the same co-ordinate system of the MR scanner. A triangularization approach was followed to obtain a surface description of the myocardial walls and the luminal surfaces of the aorta and coronary arteries suitable for importing and visualization with the mapping system.

The vertices of the endocardial and epicardial surface mesh were colour coded with the degree of transmurality for the inner and outer half of the LV wall, respectively. Meshes without colour coding were generated of the anatomy of the RV endocardial surface, the proximal aorta, and the proximal segments of the left main and right coronary artery (*Figure 1*).

Prior to the ablation procedure, all meshes were imported into the CARTO system using pre-commercial CARTO-Merge (IPE) software, enabling the registration and fusion of multiple, separate data sets.

Electrophysiological evaluation

All patients underwent electrical programmed stimulation and EAVM in the post-absorptive, non-sedated state. Antiarrhythmic drugs were discontinued for five half-lives. The protocol consisted of three drive-cycle lengths and up to three extrastimuli from two RV sites and burst pacing. The positive endpoint of stimulation was induction of a sustained monomorphic VT lasting for $>$30 s or requiring termination because of haemodynamic compromise.

Three-dimensional electroanatomical voltage mapping and image integration

Electroanatomical voltage mapping (CARTO XP) was performed during sinus or paced rhythm. Using a 3.5 mm tip, irrigated mapping catheter (NaviStar ThermoCooled, Biosense Webster Inc.) and a retrograde approach, a voltage map of the aortic root was created. Electrograms were filtered at 30–400 Hz (bipolar) and 1–240 Hz (unipolar). The catheter was positioned in the left coronary cusp and carefully advanced towards the LM. The position at the ostium

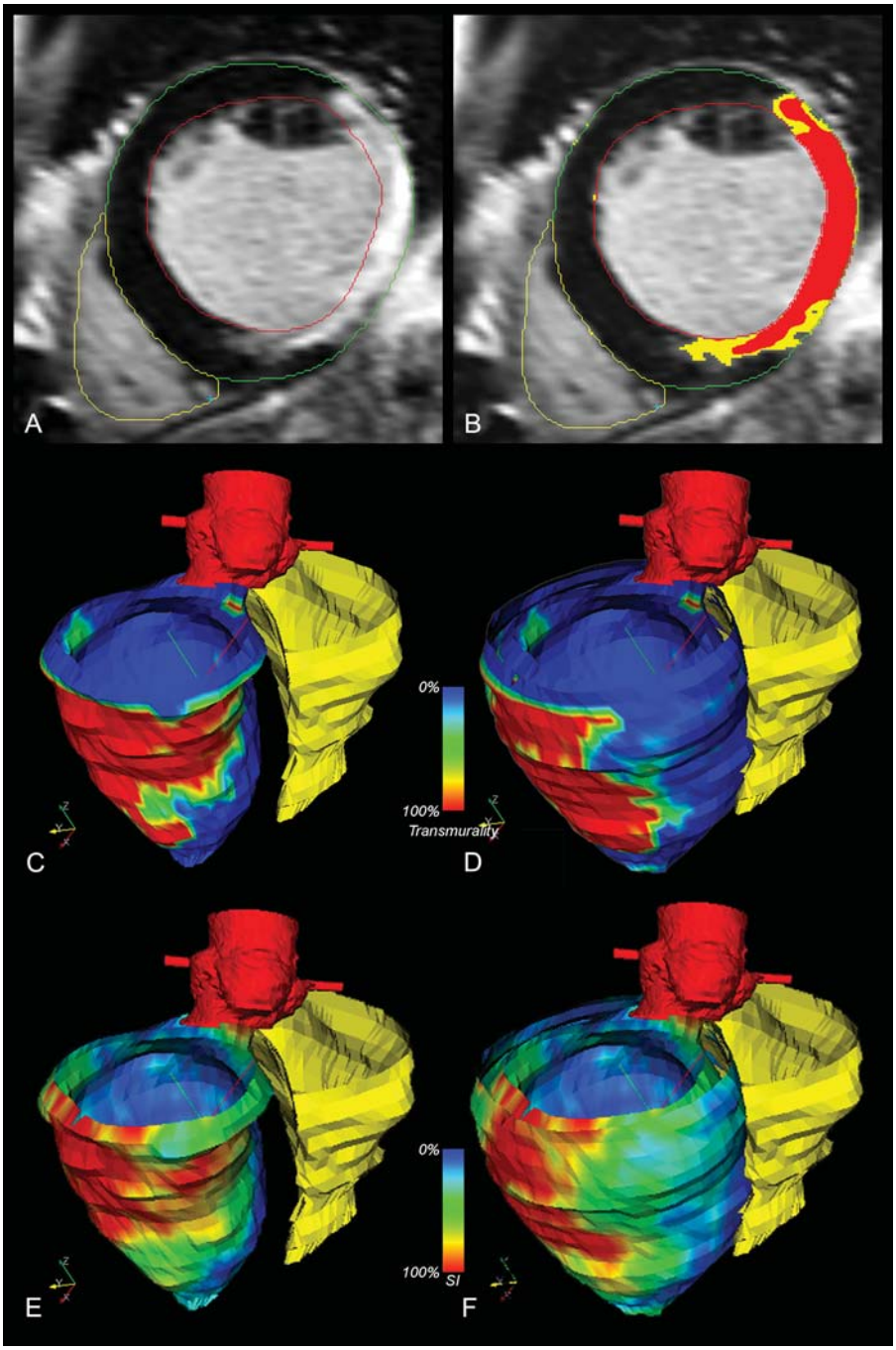

Figure 1 Pre-procedural processing consisted of drawing endo- and epicardial ventricular contours using the short-axis contrast-enhanced magnetic resonance imaging slices (*A*), defining intensity and transmurality of scar (yellow, grey zone; red, core infarction, *B*) and creating colour-coded endocardial (*C* and *E*) and epicardial (*D* and *F*) surface meshes. (C) and (D) show coding for percentage of transmurality and (E) and (F) show the same meshes coded for signal intensity according to the colour bar.

was confirmed by undiluted contrast injection through the mapping catheter. The mapping catheter was flushed with saline directly after contrast injection. Secondly, a voltage map was created of the LV. Bipolar voltages $<$1.5 mV were considered abnormal and bipolar voltages $<$0.5mV dense scar.[4,12] The pre-acquired MRI-derived meshes were integrated with the EAVM. A landmark was set at the ostium of the LM on EAVM and MRI mesh. The maps were visually aligned using the location of the LM to overcome rotation errors. Subsequently, the surface of the aortic and LV maps were automatically aligned with the meshes using CartoMERGE software (*Figure 2*). Distances between EAVM and MRI-derived maps including the LM ostium were calculated to evaluate the registration accuracy. After

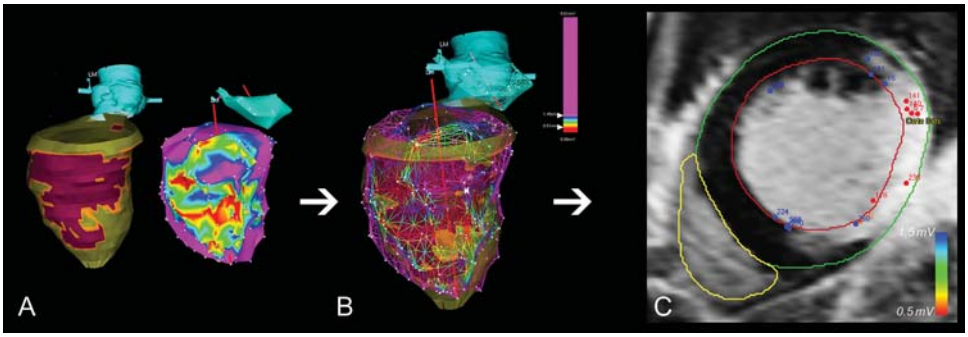

Figure 2 During the procedure, three-dimensional contrast-enhanced magnetic resonance imaging-derived meshes (purple represents scar and green represents normal myocardium) were integrated with the electroanatomical voltage maps (*A* and *B*) (colour coding as in the colour bar). After the procedure, colour-coded mapping points were superimposed on the contrast-enhanced magnetic resonance imaging slice at the corresponding location (*C*) (colour coding as in the colour bar).

registration, additional mapping points were acquired in areas with a mismatch between EAVM and MRI-derived mesh at the EA scar border zone and at areas with non-transmural scar and grey zones as assessed by CE-MRI. The location and extent of scar surface on EAVM using a cut-off value of 1.5 mV was measured using the software provided with the system and compared with the scar distribution on MRI-derived maps.

Ventricular tachycardia mapping and ablation

A VT reentry circuit isthmus site was defined by activation and entrainment mapping for tolerated VT or by pace mapping ($\geq$11/12 lead match between VT-QRS and paced-QRS morphology and stimulus-to-QRS interval $>$40 ms) for poorly tolerated VTs.[1] All isthmus sites were tagged on the EAVM and evaluated with respect to scar distribution as assessed by CE-MRI. All inducible monomorphic VTs were targeted and RF energy was applied if a potential isthmus site could be identified.

Comparison of electroanatomical voltage maps and contrast-enhanced magnetic resonance imaging

Post-procedural processing was performed in all cases. The registration matrix, mapping point co-ordinates, and bipolar and unipolar voltages were exported from the CARTO system. Using the reverse registration matrix and point co-ordinates, voltage data were superimposed on the corresponding CE-MRI slice (Mass research software, V2008-EXP) (*Figure 2C*).

To enable the assessment of voltages corresponding to different types of CE areas, each short-axis MRI slice was divided into 20 segments. Segments were subdivided into four layers (0–25, 25–50, 50–75, and 75–100% transmurality). Each layer was automatically coded as core infarct, infarct grey zone, or normal myocardium based on the mean SI. On the basis of the characteristics of the four layers, each segment was assigned to 1 of 13 subcategories discriminating between location (subendocardial, subepicardial, or mid-wall), transmurality (0, 25, 50, 75, or 100%), and SI (normal, grey-zone or core infarct) of CE scar (*Figure 3*). The bipolar and unipolar voltages of each mapping point were combined with the scar code of the CE-MRI segment at the corresponding location for analysis.

Statistical analysis

Continuous variables are expressed as mean $\pm$ SD or median (interquartile range) when appropriate, and categorical variables as frequency (%). Statistical analysis was performed using SPSS, version 16.0 (SPSS, Inc., Chicago, IL, USA). The Mann–Whitney *U*-test was used to compare voltages between different CE-MRI segment categories. All tests were two-tailed and a *P*-value of $\leq$0.05 was considered significant.

Results

Patient population

Fifteen patients (14 males, 64 $\pm$ 9 years) were studied. Patient characteristics are summarized in *Table 1*.

Delayed enhancement magnetic resonance imaging

Magnetic resonance imaging findings are listed in *Table 2*. The mean LV ejection fraction was 44 $\pm$ 10%. All patients had evidence of scar tissue on CE-MRI. The infarct was located at the anterior wall in three (20%), the inferior wall in nine (60%), and the lateral wall in three (20%) patients. The endocardial surface of segments with transmural infarction (core infarct and infarct grey zones) was 12 $\pm$ 13 cm^2 (7.7 $\pm$ 7.3% of the total surface) and of subendocardial and transmural infarctions 33 $\pm$ 20 cm^2 (23 $\pm$ 11% of the total surface). Segments with intramural or subepicardial scar accounted for 1.0 $\pm$ 0.91 cm^2 (0.74 $\pm$ 0.63%) of the total surface.

Three-dimensional electroanatomical voltage mapping and image integration

Determination of the location of the LM ostium was uncomplicated in all patients. After contrast injection, no dysfunction or obstruction of the mapping catheter was observed. Endocardial voltage maps of the aortic cusps and LV were obtained in all patients. The mean number of LV points was 255 $\pm$ 43. The imported MRI meshes were successfully merged with the aortic and LV maps with a mean surface registration error of

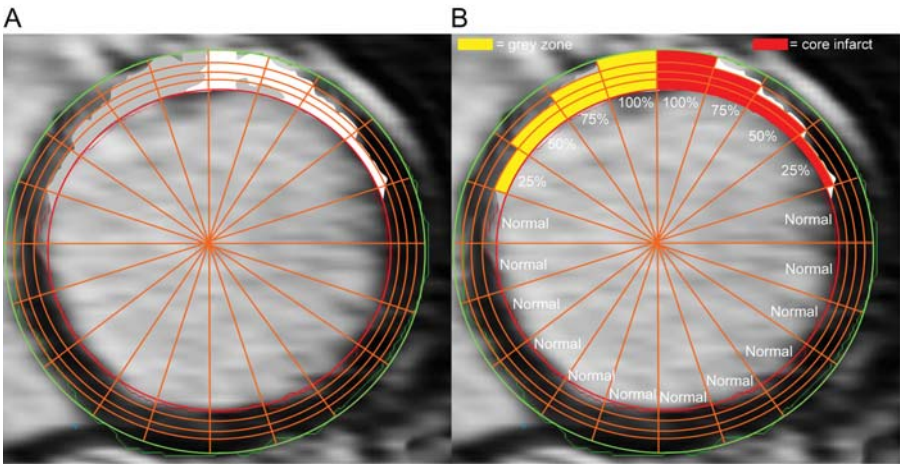

Figure 3 Schematic of the categorization of short-axis contrast-enhanced magnetic resonance imaging segments. (*A*) Potential contrast enhancement patterns with regard to transmurality and signal intensity (SI) in different segments. (*B*) The corresponding coding according to transmurality and SI (yellow, grey zone; red, core infarction).

Table 1 Patient characteristics at the time of referral for radiofrequency catheter ablation

Age	64 ± 9
Male gender (%)	14 (93)
Time after myocardial infarction (years)	14 ± 12
VT cycle length (ms)	341 ± 76
Drugs	
Amiodarone (%)	0
Sotalol (%)	1 (7)
β-Blocker (%)	14 (93)
Class I antiarrhythmic drugs (%)	1 (7)
ACE-I/AT-2 antagonist (%)	13 (87)

VT, ventricular tachycardia; ACE-I, angiotensin-converting enzyme inhibitor; AT-2, angiotensin 2. Data are expressed as mean ± SD or frequency (%).

Table 2 Results of magnetic resonance imaging studies

LV ejection fraction (%)	44 ± 10
LV end-diastolic volume (mL)	232 ± 71
LV end-systolic volume (mL)	133 ± 59
LV mass (g)	140 ± 43
Contrast-enhanced mass (g)	26 ± 20
Endocardial surface (cm^2)	134 ± 29
Transmural scar (% of surface)	7.7 ± 7.3
Subendocardial and transmural scar (% of surface)	23.0 ± 11.0
Subepicardial and mid-wall scar (% of surface)	0.7 ± 0.6
Localization contrast enhancement	
Anterior wall	3 (20)
Inferior wall	9 (60)
Lateral wall	3 (20)

LV, left ventricle. Data are expressed as mean ± SD.

3.83 ± 0.57 mm. After registration, the position error between the LM on EAVM and MRI-derived mesh was 4.64 ± 3.58 mm. Electroanatomical voltage mapping findings and registration data are summarized in *Table 3*.

Electrical infarct localization (bipolar electrograms <1.5 mV) corresponded to infarct localization on CE-MRI (≥25% transmurality) in all patients. The mean endocardial surface area of scar was 30 ± 21 cm^2 as determined by EAVM (<1.5 mV) and 33 ± 20 cm^2 as determined by CE-MRI (correlation $R = 0.91$).

However, despite this correlation, visual analysis showed a clear mismatch between EAVM scar areas and MRI maps in particular in five (33%) patients with inferior MI. In these patients, scar areas on MRI were larger than scar areas delineated by EAVM. Of importance, all scar areas not detected by EAVM were non-transmural on CE-MRI (transmurality <75%). Examples are provided in *Figure 4*.

Mapping and ablation of ventricular tachycardias

A total of 26 sustained monomorphic VTs with a cycle length of 305 ± 85ms were induced in 13 patients (1.9 ± 1.0 VTs/patient). In two patients, no sustained VT was inducible. A VT isthmus site could be identified and successfully targeted within an endocardial low-voltage area corresponding with scar on MRI for 16 VTs in nine patients. In the remaining four patients, no endocardial ablation target site could be identified. In three, the earliest activation during VT or best matching pace map was at a normal voltage site (>1.5 mV). However, at these sites, CE-MRI identified subendocardial septal scar in one and intramural inferoseptal scar in two patients. On the basis of the mapping and CE-MRI findings,

Table 3 Three-dimensional electroanatomical mapping and image integration

Mean points: aorta map	25 ± 11
Mean points: LV map	255 ± 43
Total points: LV maps	3023
Points with bipolar voltage <1.5 mV	1180 (39)
Localization low-voltage area	
Anterior	3 (20)
Inferior	9 (60)
Lateral	3 (20)
Distance: EAVM points to MRI mesh surface	
Mean (mm)	3.83 ± 0.57
Standard deviation (mm)	2.61 ± 0.49
Minimum (mm)	0.04 ± 0.04
Maximum (mm)	14.2 ± 3.36
Distance: LM EAVM to MRI mesh (mm)	4.64 ± 3.58

LV, left ventricle; EAVM, electroanatomical mapping; MRI, magnetic resonance imaging; LM, left main coronary artery. Data are expressed as mean ± SD or frequency (%).

epicardial mapping was performed in the latter with successful identification of an epicardial ablation target site. In one patient with a poorly tolerated VT, no endocardial pace match could be obtained, a mid-septal area of CE could be identified in this patient as well. Radiofrequency catheter ablation (RFCA) abolished all inducible VTs in nine, the clinical documented VT in one, and none of the clinical VTs in three patients. In two patients, ablation failed likely to the fact that there was an intramural septal reentrant circuit which was consistent with the finding of contrast enhancement at this location. In one epicardially mapped patient, no ablation was performed since the ablation target site was mapped to the close vicinity of the epicardial right coronary artery.

Ten patients received an internal cardiac defibrillator including those in whom ablation failed to abolish all VTs. The median follow-up after ablation was 19 (3–27) months during which five patients experienced recurrent VT.

Comparison of electroanatomical voltage maps and contrast-enhanced magnetic resonance imaging using reverse registration

Voltages of each mapping point were compared with the CE characteristics of the corresponding segment. One thousand five hundred and thirty-three (51%) of mapping points were allocated at a segment without CE, 1343 (44%) mapping points at a segment with subendocardial [684 (23%)] or transmural [657 (22%)] CE, and 112 (4%) of mapping points at a segment with mid-wall or subepicardial CE. The median bipolar voltage at segments with normal myocardium was 3.2 mV (1.8–5.1 mV). Endocardial bipolar electrogram amplitudes for the core infarct and infarct grey zone decreased significantly with increasing scar transmurality. The median bipolar voltages for segments with a subendocardial to transmural core infarct were 2.2 (1.1–2.5), 1.5 (0.9–2.2), 1.1 (0.6–1.7), and 0.8 (0.4–1.3) mV for 25, 50, 75, and 100% scar transmurality, respectively. For infarct grey zones, median bipolar voltages were 2.2 (1.3–3.3), 1.7 (0.8–2.4), 1.5 (0.7–2.5), and 1.0 (0.6–2.1) mV for 25, 50, 75, and 100% scar transmurality, respectively (*Figure 5*). The mean unipolar voltage was 11.5 (8.0–15.1) mV at normal segments and decreased significantly with increasing scar transmurality for core infarct and infarct grey zone. Segments with subepicardial and mid-wall scars between 25 and 75% transmurality showed reduced bipolar and unipolar electrogram voltages (*Figures 5* and *6*).

Although bipolar and unipolar electrogram amplitudes were an effective parameter to differentiate between segments of different scar transmurality, there was an important overlap between groups. A median bipolar voltage <1.5 mV was only found in segments with ≥75% core infarct transmurality and transmural grey zone infarction.

Discussion

The current study is the first to evaluate the relation between the 3D geometry of scar and local electrogram voltages using real-time integration and reversed registration of EAVM and CE-MRI in humans. The main findings of this study are: (i) real-time registration of CE-MRI-derived scar information including scar transmurality and heterogeneity and EAVM data during catheter ablation of post-MI VTs is feasible and accurate; (ii) endocardial bipolar and unipolar electrogram amplitudes decrease with increasing scar transmurality and are also influenced by scar heterogeneity as quantified by SI; (iii) the currently used bipolar electrogram cut-off value of 1.5 mV can not fully delineate non-transmural scar, small subepicardial scar, and infarct gray-zones as identified by CE-MRI.

Imaging-derived scar information and electroanatomical voltage mapping

Surviving myocyte bundles embedded in fibrous tissue are the substrate for reentrant VT in patients after MI. Identification of scar is of importance in substrate-based ablation approaches for unstable VT.[2,4] CE-MRI allows detection of small scars and characterization of infarcts by differentiating the core infarct and infarct grey-zones. The extent of the infarct grey-zone has been associated with inducible and spontaneous VT.[6–8]

Scar geometry is also an important determinant for conduction properties. The infarct border zone thickness and the local thickness gradient could predict the location of VT reentry circuit isthmuses in a canine model.[9] Thus, scar information derived from CE-MRI has the potential to improve substrate-based ablation.

The currently used gold standard in electrophysiology to define scar relies on EAVM. Two prior studies have compared CE-MRI data with EAVM in post-MI patients. In a *post hoc* analysis, a good correlation between scar areas on CE-MRI and EAVM was reported using cut-off values of 1.3 and 1.54 mV for bipolar and 5.5 and 6.52 mV for unipolar voltages, respectively.[10,11] Mismatches between the presence of scar defined by EAVM and CE-MRI found in both studies were thought to be due to the lack of high-density mapping at the scar border zone and poor catheter contact.

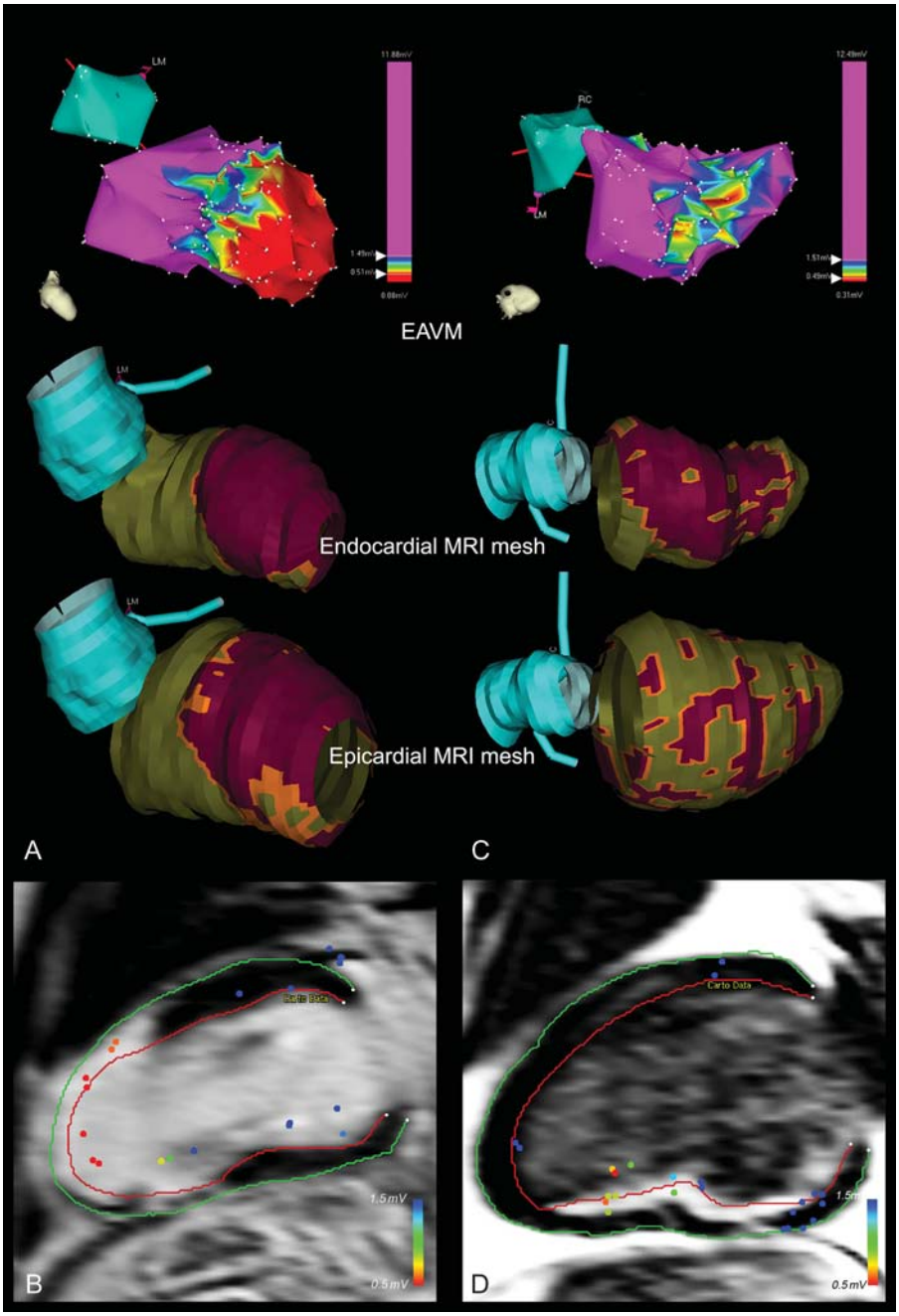

Figure 4 Representative examples of a patient in whom contrast-enhanced magnetic resonance imaging-derived mesh matched the electroanatomical voltage mapping (*A* and *B*) and of a patient with additional scar areas identified by contrast-enhanced magnetic resonance imaging not detected by electroanatomical voltage mapping (*C* and *D*). (A and C) The bipolar voltage maps (colour coding as in the colour bar) and corresponding endo- and epicardial magnetic resonance imaging-derived surface meshes coded for transmurality (purple represents scar and green represents normal myocardium). (B and D) A representative long-axis contrast-enhanced magnetic resonance imaging slice with superimposed mapping point locations (mapping point bipolar amplitudes are colour coded as in voltage maps).

Real-time integration

Real-time integration of CE-MRI-derived scar information achieved in the current study facilitated high-density mapping at the EA scar border zone and at areas with a mismatch between scar areas on EAVM and CE-MRI. The good registration accuracy prevented delineation of false-positive low-voltage areas due to poor catheter contact.

Integration of CE-MRI-derived data with EAVM was automatically performed with a mean position error of <4 mm. This accuracy is in line with studies using computed tomography

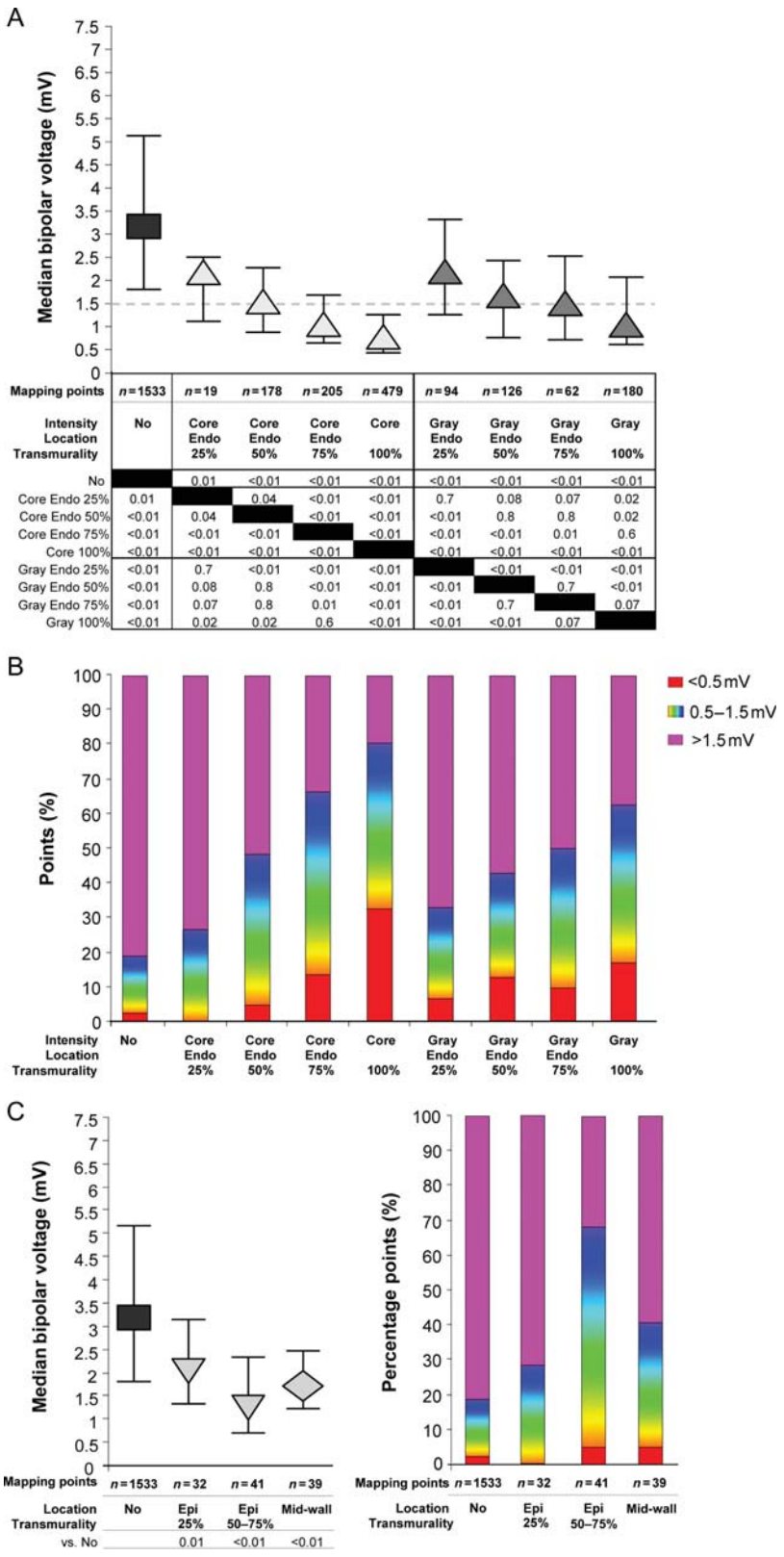

Figure 5 (*A*) Median bipolar voltage of points located at short-axis contrast-enhanced magnetic resonance imaging segments coded for transmurality and signal intensity of scar. The number of mapping points allocated at each of the nine-segment categories is provided under the *X*-axis. The *P*-value of differences (Mann–Whitney *U*-test) between bipolar voltages of each category is displayed. (*B*) The distribution of points for each segment category according to the currently used cut-off values in bipolar voltage mapping ($\leq$0.5, $>$0.5 to $\leq$1.5, and $>$1.5 mV). (*C*) The mean bipolar voltage and distribution of points at segments with epicardial and mid-wall scar.

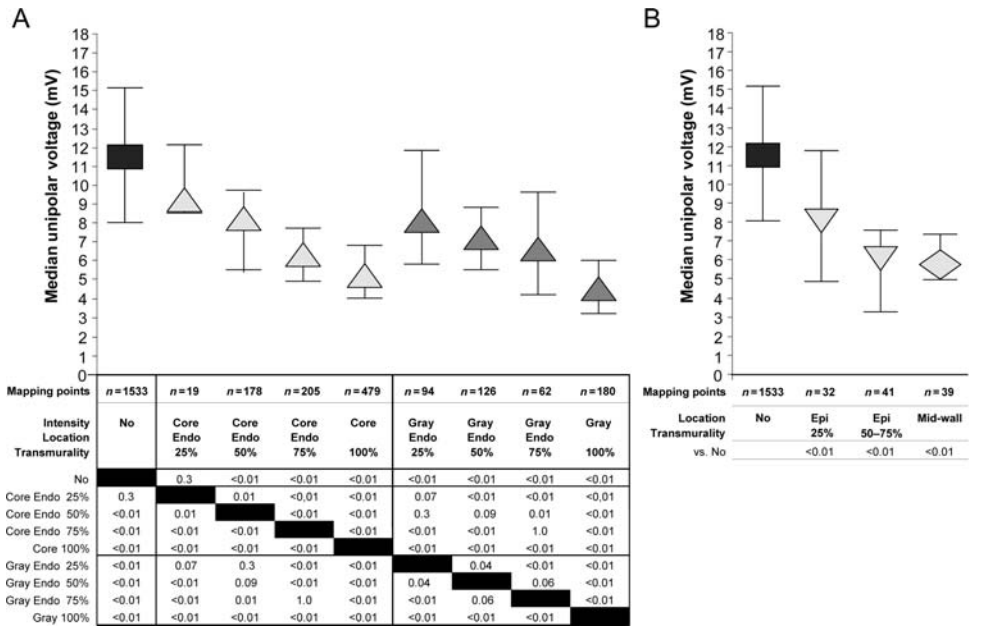

Mapping points	n=1533	n=19	n=178	n=205	n=479	n=94	n=126	n=62	n=180
Intensity Location Transmurality	No	Core Endo 25%	Core Endo 50%	Core Endo 75%	Core 100%	Gray Endo 25%	Gray Endo 50%	Gray Endo 75%	Gray 100%
No		0.3	<0.01	<0.01	<0.01	<0.01	<0.01	<0.01	<0.01
Core Endo 25%	0.3		0.01	<0.01	<0.01	0.07	<0.01	<0.01	<0.01
Core Endo 50%	<0.01	0.01		<0.01	<0.01	0.3	0.09	0.01	<0.01
Core Endo 75%	<0.01	<0.01	<0.01		<0.01	<0.01	<0.01	1.0	<0.01
Core 100%	<0.01	<0.01	<0.01	<0.01		<0.01	<0.01	<0.01	<0.01
Gray Endo 25%	<0.01	0.07	0.3	<0.01	<0.01		0.04	<0.01	<0.01
Gray Endo 50%	<0.01	<0.01	0.09	<0.01	<0.01	0.04		0.06	<0.01
Gray Endo 75%	<0.01	<0.01	0.01	1.0	<0.01	<0.01	0.06		<0.01
Gray 100%	<0.01	<0.01	<0.01	<0.01	<0.01	<0.01	<0.01	<0.01	

Mapping points	n=1533	n=32	n=41	n=39
Location Transmurality	No	Epi 25%	Epi 50–75%	Mid-wall
vs. No		<0.01	<0.01	<0.01

Figure 6 (*A*) Median unipolar voltage of points located at short-axis contrast-enhanced magnetic resonance imaging segments coded for transmurality and signal intensity of scar. The number of mapping points allocated at each of the nine-segment categories is provided under the *X*-axis. The *P*-value of differences (Mann–Whitney *U*-test) between mean unipolar voltages of each category is displayed. (*B*) Median unipolar voltage of points at segments with epicardial and mid-wall scar.

imaging.[13,14] In contrast to prior studies in which the position of LV apex, mitral annulus, and aorta was used for registration, we tagged the position of the LM ostium. The advantage of using the LM and endocardial surface registration is that it precludes rotation errors.[15]

After image integration and delineation of the EA border zone, we found a good correlation between the surface of scar measured by EAVM using a cut-off value of 1.5 mV and scar surface area derived from CE-MRI. However, visual analysis showed a clear mismatch between scar areas defined by EAVM and the area of scar coded on the CE-MRI meshes. CE-MRI scar areas were larger in 33% of the patients. Insufficient mapping density was excluded as a cause of the mismatch by acquiring additional mapping points in these areas after image integration.

The surface of low-voltage areas was measured using the CARTO software. This software sums the surface of all individual triangles between mapping points. Therefore, the total surface increases with the number of mapping points that are not located in the same plane. Comparing the absolute endocardial scar surface calculated by using the CARTO system with the scar surface measured by the endocardial contours on CE-MRI might therefore be inaccurate.

Reversed registration

The newly proposed technique of reversed registration allowed a head-to-head comparison of voltage data and CE-MRI characteristics, independent of surface measurements.

Bipolar and unipolar electrogram amplitudes significantly decreased with increasing scar transmurality for core infarct and infarct grey zones. A similar correlation between decreasing bipolar voltages and increasing scar transmurality assessed by histology was demonstrated in a dog model of MI.[16] For segments with ≥75% scar transmurality, bipolar electrograms were also significantly influenced by scar density defined by SI. Interestingly, the only segments with a median bipolar voltage of <1.5 mV were segments coded as ≥75% transmural core and completely transmural grey zone infarction (*Figure 5*).

This finding is in line with prior animal studies as transmural scars are the prevailing type of scar found in pigs after MI in which the cut-off value of 1.5 mV was validated.[12] In the current study performed in patients with a relatively preserved LV function, however, transmural scars accounted for only 7.7% of the total endocardial surface. Forty-four per cent of all mapping points located at a scar area were allocated to a segment with <75% transmural core or infarct grey zone. The variation in number, size, and geometry of surviving myocyte bundles in non-transmural and inhomogeneous scar are likely to influence local electrogram amplitudes.

Accordingly, non-transmural and inhomogeneous scars showed significant higher bipolar and unipolar voltages contributing to the mismatch between EAVM and CE-MRI-derived scar maps after image integration and visual comparison.

The total subendocardial surface of segments with only mid-wall or subepicardial scar was small, which might be expected in a post-MI population.

Defining a voltage cut-off value for the presence of scar, based on real-time image integration as suggested by others,[10,11,13] is appealing. However, due to the demonstrated complex relation between

local electrogram amplitudes and scar characteristics, a single cut-off value cannot discriminate between the presence and the absence of infarct scar at a particular location, because voltage is dependent on infarct transmurality and heterogeneity.

Reentry circuit isthmus sites and scar characteristics

It has been demonstrated that in patients with haemodynamically tolerated VT, the majority of successful ablation sites were located in the EA scar border zone using a cut-off value of 1.5 mV. However, some ablation sites were located within the normal myocardium as defined by EAVM.[17]

More recently, Desjardins *et al.* reported that VT isthmus sites, the majority identified by pace mapping, had a mean bipolar voltage of 0.6 ± 0.9 mV and corresponded to core infarct regions or transmural grey zones on CE-MRI using post-procedural image integration. Of importance, for one-third of the induced VT, no isthmus could be identified.[10]

In the current study, we were unable to identify a VT reentry isthmus site within a low-voltage area in four patients. However, in three patients, successful identification of an ablation target site was guided by CE-MRI-derived scar information showing non-transmural scar leading to pace mapping in a normal voltage area in one and an epicardial ablation attempt in two patients.

Clinical implications

Real-time integration of CE-MRI-derived scar maps and EAVM is feasible and accurate. Of importance, all CE-MRI information including the location of intramural and non-transmural scar and of the core infarct and infarct grey zone not detectable by EAVM can be visualized during the ablation procedures. This might have important implications for substrate-based ablation procedures in particular in patients, in whom variation in collateral circulation and early reperfusion strategies have resulted in inhomogeneous and non-transmural infarction. The technique of reversed registration as described in this study may also provide more insights into the spatial relationship between VT reentry circuit sites and scar characteristics on CE-MRI as successful ablation sites can be superimposed on the CE-MRI.

Limitations

The studied population consisted of post-MI patients without contraindications for MRI study. The routine use of MRI in ICD carriers is not considered safe and currently limits the application of the described methods. The increasing availability of 'MRI-safe' implantable defibrillators in the near future may however make the use of MRI-derived information during RFCA applicable to a larger population.

The sample size of the patient population included in this study was relatively small. Further studies in larger groups of patients are warranted to further study the supplemental value of the integration of MRI-derived scar information during VT ablation.

Conclusions

Real-time integration of CE-MRI-derived scar information including scar transmurality and heterogeneity and EAVM data during catheter ablation of post-MI VTs is feasible and accurate.

Electrogram voltages decrease with increasing scar transmurality and are also influenced by scar heterogeneity. The currently used bipolar voltage cut-off value of 1.5 mV seems to be appropriate to delineate transmural scar. However, local bipolar and unipolar voltages alone are not sufficient to characterize the complex 3D scar geometry. Merging CE-MRI-derived information with EAVM provides supplementary substrate information in particular for non-transmural and heterogeneous infarction.

Funding

This study is supported by the Netherlands Heart Foundation (grant 2008B074).

Conflict of interest: none declared.

References

1. Aliot EM, Stevenson WG, Almendral-Garrote JM, Bogun F, Calkins CH, Delacretaz E, Della BP, Hindricks G, Jais P, Josephson ME, Kautzner J, Kay GN, Kuck KH, Lerman BB, Marchlinski F, Reddy V, Schalij MJ, Schilling R, Soejima K, Wilber D. EHRA/HRS Expert Consensus on Catheter Ablation of Ventricular Arrhythmias: developed in a partnership with the European Heart Rhythm Association (EHRA), a Registered Branch of the European Society of Cardiology (ESC), and the Heart Rhythm Society (HRS); in collaboration with the American College of Cardiology (ACC) and the American Heart Association (AHA). *Heart Rhythm* 2009;**6**:886–933.
2. Soejima K, Suzuki M, Maisel WH, Brunckhorst CB, Delacretaz E, Blier L, Tung S, Khan H, Stevenson WG. Catheter ablation in patients with multiple and unstable ventricular tachycardias after myocardial infarction: short ablation lines guided by reentry circuit isthmuses and sinus rhythm mapping. *Circulation* 2001;**104**:664–669.
3. Stevenson WG, Wilber DJ, Natale A, Jackman WM, Marchlinski FE, Talbert T, Gonzalez MD, Worley SJ, Daoud EG, Hwang C, Schuger C, Bump TE, Jazayeri M, Tomassoni GF, Kopelman HA, Soejima K, Nakagawa H. Irrigated radiofrequency catheter ablation guided by electroanatomic mapping for recurrent ventricular tachycardia after myocardial infarction: the multicenter thermocool ventricular tachycardia ablation trial. *Circulation* 2008;**118**:2773–2782.
4. Marchlinski FE, Callans DJ, Gottlieb CD, Zado E. Linear ablation lesions for control of unmappable ventricular tachycardia in patients with ischemic and non-ischemic cardiomyopathy. *Circulation* 2000;**101**:1288–1296.
5. Kim RJ, Fieno DS, Parrish TB, Harris K, Chen EL, Simonetti O, Bundy J, Finn JP, Klocke FJ, Judd RM. Relationship of MRI delayed contrast enhancement to irreversible injury, infarct age, and contractile function. *Circulation* 1999;**100**:1992–2002.
6. Wagner A, Mahrholdt H, Holly TA, Elliott MD, Regenfus M, Parker M, Klocke FJ, Bonow RO, Kim RJ, Judd RM. Contrast-enhanced MRI and routine single photon emission computed tomography (SPECT) perfusion imaging for detection of subendocardial myocardial infarcts: an imaging study. *Lancet* 2003;**361**:374–379.
7. Schmidt A, Azevedo CF, Cheng A, Gupta SN, Bluemke DA, Foo TK, Gerstenblith G, Weiss RG, Marban E, Tomaselli GF, Lima JA, Wu KC. Infarct tissue heterogeneity by magnetic resonance imaging identifies enhanced cardiac arrhythmia susceptibility in patients with left ventricular dysfunction. *Circulation* 2007;**115**:2006–2014.
8. Roes SD, Borleffs CJ, van der Geest RJ, Westenberg JJ, Marsan NA, Kaandorp TA, Reiber JH, Zeppenfeld K, Lamb HJ, DE RA, Schalij MJ, Bax JJ. Infarct tissue heterogeneity assessed with contrast-enhanced MRI predicts spontaneous ventricular arrhythmia in patients with ischemic cardiomyopathy and implantable cardioverter-defibrillator. *Circ Cardiovasc Imaging* 2009;**2**:183–190.
9. Ciaccio EJ, Ashikaga H, Kaba RA, Cervantes D, Hopenfeld B, Wit AL, Peters NS, McVeigh ER, Garan H, Coromilas J. Model of reentrant ventricular tachycardia based on infarct border zone geometry predicts reentrant circuit features as determined by activation mapping. *Heart Rhythm* 2007;**4**:1034–1045.
10. Desjardins B, Crawford T, Good E, Oral H, Chugh A, Pelosi F, Morady F, Bogun F. Infarct architecture and characteristics on delayed enhanced magnetic resonance

imaging and electroanatomic mapping in patients with postinfarction ventricular arrhythmia. *Heart Rhythm* 2009;**6**:644–651.
11. Codreanu A, Odille F, Aliot E, Marie PY, Magnin-Poull I, Andronache M, Mandry D, Djaballah W, Regent D, Felblinger J, De Chillou C. Electroanatomic characterization of post-infarct scars comparison with 3-dimensional myocardial scar reconstruction based on magnetic resonance imaging. *J Am Coll Cardiol* 2008;**52**:839–842.
12. Reddy VY, Wrobleski D, Houghtaling C, Josephson ME, Ruskin JN. Combined epicardial and endocardial electroanatomic mapping in a porcine model of healed myocardial infarction. *Circulation* 2003;**107**:3236–3242.
13. Dickfeld T, Lei P, Dilsizian V, Jeudy J, Dong J, Voudouris A, Peters R, Saba M, Shekhar R, Shorofsky S. Integration of three-dimensional scar maps for ventricular tachycardia ablation with positron emission tomography-computed tomography. *JACC Cardiovasc Imaging* 2008;**1**:73–82.
14. Bogun FM, Desjardins B, Good E, Gupta S, Crawford T, Oral H, Ebinger M, Pelosi F, Chugh A, Jongnarangsin K, Morady F. Delayed-enhanced magnetic resonance imaging in nonischemic cardiomyopathy: utility for identifying the ventricular arrhythmia substrate. *J Am Coll Cardiol* 2009;**53**:1138–1145.
15. Zeppenfeld K, Tops LF, Bax JJ, Schalij MJ. Images in cardiovascular medicine. Epicardial radiofrequency catheter ablation of ventricular tachycardia in the vicinity of coronary arteries is facilitated by fusion of 3-dimensional electroanatomical mapping with multislice computed tomography. *Circulation* 2006;**114**:e51–e52.
16. Wolf T, Gepstein L, Dror U, Hayam G, Shofti R, Zaretzky A, Uretzky G, Oron U, Ben-Haim SA. Detailed endocardial mapping accurately predicts the transmural extent of myocardial infarction. *J Am Coll Cardiol* 2001;**37**:1590–1597.
17. Verma A, Marrouche NF, Schweikert RA, Saliba W, Wazni O, Cummings J, Abdul-Karim A, Bharqava M, Burkhardt JD, Kilicaslan F, Martin DO, Natale A. Relationship between successful ablation sites and the scar border zone defined by substrate mapping for ventricular tachycardia post-myocardial infarction. *J Cardiovasc Electrophysiol* 2005;**16**:465–471.